$4n^2$ Absorption and < 1% Spectrum-and-Angle-Averaged Reflection in High Lifetime Tapered Microwire Arrays

Sisir Yalamanchili[1,3†], Hal S. Emmer[1,†], Katherine T. Fountaine[2,6], Christopher T. Chen[1], Nathan S. Lewis[2-5*], and Harry A. Atwater[1,3,4]

[1]Division of Engineering and Applied Sciences, California Institute of Technology, Pasadena, CA 91125
[2]Division of Chemistry and Chemical Engineering, California Institute of Technology, Pasadena, CA 91125
[3]The Joint Center for Artificial Photosynthesis, California Institute of Technology, Pasadena, CA 91125
[4]Kavli Nanoscience Institute, California Institute of Technology, Pasadena, CA 91125
[5]Beckman Institute, California Institute of Technology, Pasadena, CA 91125
[6]NGNext, Northrop Grumman Aerospace Systems, 1 Space Park Dr., Redondo Beach, CA 90278

[†]These authors contributed equally
*Corresponding Author: haa@caltech.edu

ABSTRACT

We report ordered, high aspect ratio, tapered Si microwire arrays that exhibit an extremely-low angular (0^o to 50^o) and spectrally averaged reflectivity of <1% of the incident 400 nm - 1100 nm illumination. After isolating the microwires from the substrate with a polymer infill and peel off process, the arrays were found to absorb 89.1% of angular averaged incident illumination (0^o to 50^o) in the equivalent volume of a 20 micron thick Si planar slab, reaching 99.5% of the classical light trapping limit between 400 nm - 1100 nm. We explain the broadband absorption by enhancement in coupling to waveguide modes due to the tapered microstructure of the arrays. Time-resolved microwave photoconductivity decay measurements yielded charge-carrier lifetimes of 0.75 μs in the tapered microwires resulting in an implied V_{oc} of 0.655 V. The high absorption, long charge-carrier lifetimes, and high aspect ratio in these ordered microwire arrays make them an attractive platform for high efficiency thin-film crystalline Si solar cells and as well as for the photoelectrochemical production of fuels from sunlight.

Keywords: Silicon, Microwires, Reflection, Absorption, Waveguide, ICPRIE, Carrier Lifetime, Surface Passivation

Reaching towards the ultimate conversion efficiency limits for Si photovoltaics is of considerable fundamental and practical interest, and motivates research on thin Si solar cells with high minority carrier lifetimes and extremely efficient light management. While the limiting efficiency [1] for a single-junction crystalline Si solar cell under 1 sun illumination of 29.8% constrained only by free carrier and Auger absorption losses [2], record experimental Si cells have reached efficiencies as high as 25.6%[3]. To achieve higher efficiencies, lower surface recombination velocities must be achieved in structures with very efficient light management that enable a reduced bulk recombination by virtue of reduced absorber volume in the solar cell. Current high-efficiency Si solar cells utilize intrinsic amorphous silicon (i-a-Si) [4]or Al_2O_3 [5] surface passivation layers that produce very low surface recombination velocities, so that the cell performance is typically limited by the bulk carrier lifetime. Consequently, a further decrease in bulk recombination could lead to yet higher cell efficiencies. Heterostructure with intrinsic thin layer (HIT) Si solar cells have demonstrated an efficiency enhancement by the use of thinner substrates [4]. In such HIT cells, the dark current due to recombination is reduced compared to the current under illumination, increasing the quasi-Fermi level. Use of even thinner substrates would be desirable in order to reduce the bulk recombination volume, but the indirect band gap of Si yields reduced absorption in very thin samples. Additionally, the surface/bulk ratio increases as the substrate becomes thinner. The optimal Si cell thickness thus depends strongly on the achievable surface recombination velocities as well as on the ability to achieve enhancements in light trapping. Optoelectronic transport calculations indicate that with realistic surface recombination velocities, and high bulk material quality, efficiencies as high as 24.4% could be achieved in a 10 μm thick cell [6] if the light trapping were at the $4n^2$ Lambertian limit [7]. Previous demonstrations of thin film crystalline Si cells with effective thickness under 50 μm with various light trapping schemes

include: 20.62% efficiency in a 35μm device[3], 19.1% in a 43μm thick device [8], 16.8% in a 20μm thick device [9], 15.7% [10] and 13.7% [11] in 10μm thick devices .

Various nanostructured antireflection and light-trapping strategies have been explored for thin-film crystalline Si [12] [13]. Some recent studies have shown limitations in light-trapping structures arising from parasitic absorption, as opposed to limitations in the Si absorber material of the cell. Hence structuring the absorber layer to maximally harvest light while minimizing parasitic absorption and reflection losses, is required to maximize absorption in thin crystalline Si solar cells [14]. Si microwire arrays facilitate light absorption near the $4n^2$ limit for very small Si planar equivalent thicknesses, [15] with reports of absorption exceeding the $4n^2$ limit near the band edge. However to date, Si microwires fabricated by vapor- liquid-solid growth methods using metals such as Au or Cu as growth catalysts have not demonstrated high minority carrier recombination lifetimes, since these metals can produce defects that reduce the bulk recombination lifetime in Si [16] [17].

We demonstrate here that Si microwires with high minority carrier bulk lifetimes can be fabricated by cryogenic inductively coupled plasma reactive ion etching (ICPRIE), which is predominantly a chemical etch, and demonstrate that the etching conditions can be modified to taper the Si microwire shape to achieve high aspect ratio arrays with near $4n^2$ light trapping and extremely low angle- and spectrally-averaged low reflectivities. Electrodynamic simulations indicate that the tapered Si microwire structure facilitates highly effective coupling of incident light into waveguide modes, and yield high optical absorption.

High aspect ratio pillar structures with high precision have been fabricated in Si wafers by a cryogenic ICPRIE for various solid state device applications [18]. Aluminum oxide (Al_2O_3) is a nearly ideal etch mask with nearly 1:1000 selectivity, which can be used to achieve structures with

high aspect ratios as high as 20:1 [19]. The high aspect ratio tapered microwire arrays shown in Fig. 1a are fabricated from high lifetime (>1ms) float zone grown Si wafers via photolithography followed by ICPRIE and standard Si surface cleaning methods [20]. The resulting structure features wires with tip radius of curvature of 25 nm, bottom base diameter of 7 μm, and a height of 75 μm, in a square lattice with 7 μm pitch.

Angle-dependent reflectance measurements were performed using tunable monochromatic radiation from a supercontinuum laser and a Si photodetector [15]. Figures 1b and 1c show the measured wire array reflectance on linear and log scales, respectively, from 400 nm – 1100 nm, while the angle was varied from 0^0 to 50^o. Averaged over 0^o to 50^o and over the range 400 nm-1100 nm, the integrated reflectance was 0.98% for uncoated Si wire arrays and 0.97% for arrays coated with SiN_x dielectric layers. The tapered microwire arrays thus act as nearly ideal antireflection surfaces, not only at normal incidence but also at oblique incidence angles even without any anti reflection coating. The angular reflectance without and with SiN_x anti reflection coating is shown in Fig. 1c, and d and Fig. 1e, and f respectively in linear and log plots. The surface reflectance is comparable- -and in some cases lower than-- typical black Si front-surface texturing methods [21] [22] [23]. Notably, low reflection was achieved at wavelengths near the Si band gap, i.e., 1000 nm – 1100 nm, where Si has a large absorption length. In the 1000 nm – 1100 nm wavelength range, the reflection varied from 3.6% at normal incidence to 2.7% at 50^o for uncoated wires, which may be limited by reflection from back surface of the sample. In the 400 nm – 1000 nm range, the reflection varied from 0.7% - 0.5%. Although not all previous work has reported angular averages for reflectance, the present result of <1% angular averaged reflection is to our knowledge a record for low reflectance silicon structures, and compares very favorably to other

methods for reducing reflection in the range 400 nm – 1100 nm, the wavelength range of interest for Si-based solar cells.

In order to experimentally measure absorption in tapered microwire arrays without effects due to the substrate, the uncoated arrays were embedded in polydimethylsiloxane (PDMS), by spin coating followed by curing such that Si microwires were completely embedded in the polymer. The arrays were peeled off of their substrate using a razor blade, to produce flexible films with embedded Si microwires [24-25]. These films were placed on a nearly ideal Lambertian back scattering $BaSO_4$ (6080 White Reflectance Coating; LabSphere) coated sample holder in an integrating sphere, and reflection (R) measurements were performed. The absorption (A) was calculated from the reflectance (R) data by using $A = 1 - R$. Fig. 2a and 2b show the peeled off PDMS films with embedded, tapered Si microwire arrays. Fig. 2c shows the absorption calculated from the reflection measurement in the integrating sphere from 400 nm – 1100 nm while the angle was varied from 0^o to 50^o. Averaged over 0^o to 50^o, such films showed an integrated absorbed solar spectrum photon flux as high as 89.1%, demonstrating the remarkable absorption properties of these tapered microwire arrays at various incident angles in the solar spectrum of interest. The effective planar thickness of these polymer-embedded arrays calculated assuming a truncated cone with tip radius of 25 nm, base radius of 3.5 μm, and a height of 70 μm is ~20 μm. Fig. 2d shows a comparison of the absorbed solar flux under normal incidence to the $4n^2$ light -trapping limit [26] for a 20 μm thick Si slab, after correcting for reflection from the PDMS/air interface (~3%). The total calculated photon flux absorbed at normal incidence was 99.5% of the limit for an equivalent thick Si slab. The absorption was slightly below the $4n^2$ limit for most of the solar spectrum, and exceeded the limit at wavelengths near the Si band gap (1050 nm – 1100 nm). Fig. 3 shows angular averaged reflection from Si substrate with tapered microwires etched into in red,

and angular averaged absorption in tapered microwire arrays embedded in PDMS in blue plotted in 400 nm – 1100 nm wavelength range, summarizing the reflection and absorption measurements.

The exceptionally low reflectivity of the arrays arises from the tapered wire geometry. The fill fraction of the arrays at the light-incident interface is less than 0.01% and increases extremely gradually along the extended length of the tapered microwires. The remarkable optical characteristics – minimal reflection and high absorption-- of the tapered Si microwire arrays cannot be completely explained by either effective medium concept or ray optic analysis especially at wavelengths near band gap of Si, and requires a wave-optical analysis for quantification. From this, the measured absorption is seen in this case to arise from efficient coupling of incident light into waveguide modes in the wires. We employed a combination of full wave electromagnetic simulations and analytic waveguide analysis to develop an understanding of the array optical properties. The strong symmetry overlap of specific waveguide modes also contributes to the low reflectivity, and is discussed in more detail below. Bloch modes, which often result in reflection bands,[27,28,29] play an insignificant role in these structures due to an inter wire spacing that is much larger than the optical wavelength. Consequently, each tapered microwire acts as an independent optical antenna and waveguide, consistent with previous findings [30,31,32].

The high absorption arises from a combination of coupling into waveguide modes and the length of the microwires. Many groups have studied and demonstrated enhanced absorption in Si nanowire arrays due to coupling into waveguide modes with large extinction cross sections.[33,34,35,36] However even with careful optical design, Si nanowire array absorption have smaller absorption than for planar Si absorbers, owing to the indirect gap and consequent low absorption coefficient of Si. Our microwire structures also capitalize on waveguide modes for

optical absorption enhancement, while simultaneously incorporating long optical path lengths to achieve near-unity absorption. Efficient coupling into the optical waveguide modes of the Si microwires is the critical factor in the remarkable optical properties of these arrays.

Three-dimensional full field electromagnetic wave simulations of tapered microwire arrays were performed to characterize the waveguide modes. The simulation procedure is explained in detail in the methods section. Fig. 4 displays carrier generation cross-sections for tapered microwires at incident wavelengths of 400, 600, 800, and 1000 nm, respectively. Fig. 4 e-h show complete wire cross sections on a logarithmic scale, marked with light blue squares indicating the bounds of Fig. 4 a-d, which focus on the upper portion of the wire and are shown in linear scale. All absorption profiles indicate light coupling into waveguide modes, but the modes are less obvious at λ=400nm (Fig. 4a and 4e), due to strong absorption above the direct gap of Si. Below the direct gap of Si, the waveguide characteristics become more apparent. Absorption occurs primarily in the microwire core, indicative of guided mode propagation in the wire, and exhibits semi-periodic longitudinal intensity oscillations that scale with incident wavelength, indicative of mode propagation. Additionally, the existence of significant intensity near the lower end of the microwire in the λ=1000 nm profile demonstrates long distance waveguide mode propagation to the bottom of the microwire, enabling near-unity absorption for wavelengths near the Si band edge. Simulations show that the reflection is <1% at wavelengths below 1000 nm agreeing with the measurements.

Detailed mode analysis reveals that light couples into the set of first azimuthal order waveguide modes, HE_{1n}, as illustrated for λ=1000nm illumination in Fig. 5. As previously reported,[37,38] efficient coupling occurs into this set of modes due to the strong overlap in symmetry between the incident plane wave and the in-plane mode field profiles. Fig. 5a displays a longitudinal cross

section marked with horizontal dashed lines colored to indicate their correlation with the radial cross sections in Fig. 5b-g; the radial cross sections correspond to the first six HE_{1n} modes, in ascending order. As expected, the first order HE_{11} mode appears at the top of the wire, and the higher order modes appear in sequence, as radius increases.

$$\left(\frac{1}{k_{cyl}^2}-\frac{1}{k_{out}^2}\right)^2\left(\frac{\beta m}{k_0 a}\right)^2=\left(\frac{\varepsilon_{r,cyl}\mu_{r,cyl}}{k_{cyl}}\frac{J_m'\left(k_{cyl}a\right)}{J_m\left(k_{cyl}a\right)}-\frac{\varepsilon_{r,out}\mu_{r,out}}{k_{out}}\frac{H_m'\left(k_{out}a\right)}{H_m\left(k_{out}a\right)}\right)\left(\frac{1}{k_{cyl}}\frac{J_m'\left(k_{cyl}a\right)}{J_m\left(k_{cyl}a\right)}-\frac{1}{k_{out}}\frac{H_m'\left(k_{out}a\right)}{H_m\left(k_{out}a\right)}\right) \quad (2)$$

The dispersion curves for these modes were calculated from the eigenvalue equation (Eqn. 2) for cylindrical dielectric waveguides,[39] where J_m and H_m are the cylindrical Bessel and Hankel functions of the mth order, k_0 is the free space wavevector, k_{cyl}(k_{out}) is the transverse wavevector inside(outside) the cylinder, β is the mode propagation constant, $\varepsilon_{r,cyl}$ ($\varepsilon_{r,out}$) and $\mu_{r,cyl}$($\mu_{r,out}$) are the relative dielectric permittivity and permeability inside(outside) the cylinder, and a is the cylinder radius. Fig. 5h and Fig. 5i show the dispersion curve for a Si waveguide (n=3.577), in its tradition form, k_0a(βa), and a non-traditional form, mode index vs. radius, respectively. The mode color key in Fig. 5h is consistent throughout the figure. The dashed lines on Fig. 5i indicate the radius of the mode cross sections in Fig. 5b-g, revealing that the modes are most prominent between a mode index of 1 and 2. This moderate mode index is due to a tradeoff between ease of free space coupling and mode confinement mediated-absorption. Mode profiles, propagation constants and radius range are all consistent with analytic waveguide theory. These observations demonstrate the critical role of waveguide modes in the optical characteristics of the tapered microwire arrays.

In order to evaluate quality of tapered microwires and estimate the V_{oc}, transmission electron microscopy (TEM) and lifetime measurements were performed. Electron microscopy images of the sidewall shown in the Fig. S1 (see supplementary information) shows minimal surface damage due to etching, and no lattice damage in the bulk, as expected from the low forward power (5W)

and predominantly chemical nature of the dry etching process. The carrier recombination lifetimes were measured for tapered microwire arrays passivated by Al_2O_3 coated-microwires by atomic layer deposition (ALD) [5, 40] using a custom-built microwave photoconductive decay lifetime tool with a Nd:YaG laser illumination source operating at 1064 nm. 30-120 µJ energy pulses of 5 ns and spot size of 3 mm diameter at 50 Hz frequency were used for these measurements, as illustrated in Fig. S2 (see supplementary information). The cleaning process steps and the measurement technique of these tapered microwires are detailed in the methods section. Al_2O_3 passivated tapered microwire arrays were embedded in PDMS and peeled from their respective substrates using a razor blade. During the measurements, the fractured back surfaces of the peeled microwires were passivated *in situ* using 5.8M HCl, after a 20s damage removal etch in 3.6M KOH at room temperature. Lifetimes of 0.75 µs were measured in these arrays. An analytical model was implemented to estimate surface recombination velocity (SRV), implied V_{oc}, and the corresponding maximum efficiency achievable from the carrier lifetime measurements. The SRV achieved was estimated to be 150 cm/s, with the corresponding implied V_{oc} to be 0.655 V, and the maximum efficiency achievable to be 22.2%. The model is described in detail in the Methods section. The tapered microwire arrays are surface recombination limited and a further decrease in SRV to 5 cm/s is shown to enhance the lifetime to > 15 µs, and the maximum achievable efficiency to > 25%.

In conclusion, the tapered microwire arrays fabricated in this work demonstrate superior light trapping properties with <1% angular averaged reflection, and absorption reaching the $4n^2$ light trapping limit due to enhanced coupling of incident light into the waveguide modes. These microwires show no bulk damage and minimal surface damage that can be removed by surface cleaning after fabrication. We measured carrier lifetime in these microstructures by microwave

detected photoconductivity measurement, and measured lifetimes of $0.75\ \mu s$ for wires under ALD deposited 20 nm thick Al_2O_3 sidewall passivation with 5.8M HCl back surface passivation. In this work the performance of the arrays is limited by surface recombination and therefore further improvement in surface passivation methods to these arrays can push the performance of these arrays to reach $V_{oc} > 0.7$ V and maximum possible efficiency > 25%. Future devices using these tapered microwire arrays can be envisioned, such as all back contact solar cells [5, 11, 40-41] similar to previous demonstrations with an ultrathin Si substrate [42] or as a flexible solar cell with a convention back contact and a transparent front contact [25]. Due to the high surface area and superior light trapping these tapered microwires are also excellent candidates for applications in photoelectrochemical cells and enhancing electrode efficiencies [43].

METHODS

Fabrication of tapered microwire arrays: High lifetime (> 1ms) FZ grown Si wafers were photolithographically patterned into a square grid with 3μm circles of 200nm thick Al_2O_3 mask evaporated over it separated by 7μm. SF_6/O_2 etch chemistry was used in Oxford DRIE System 100 ICP/RIE to perform the etching. Etching was performed at low capacitive coupled power of 5W to reduce damage due to momentum of ions. A high inductively coupled power of 900 W was used to increase the number of ions in the plasma to reach high rates of chemical etch. During etch the SF_6/O_2 ratio was increased from 70 sccm/5 sccm to 70 sccm/6 sccm in steps of 0.5 sccm of O_2 every 30min. The chamber was maintained at a temperature of -120 ^oC and a pressure of 10 mTorr during the etching process. Post etching the wafers were dipped in buffered hydrofluoric acid solutions to etch away the Al_2O_3 mask. The samples were then cleaned using modified RCA1 and RCA2 cleaning processes [20]. SiN_x was deposited over the Si wire substrates by plasma

enhanced chemical vapor deposition (PECVD) using an Oxford Instruments Plasmalab System 100. Silane and ammonia gas chemistry was used at 350 ^{o}C and 1 torr at previously optimized conditions for microwire arrays [15].

Sample preparation for absorption measurements:

Tapered microwire arrays were embedded in Polydimethylsiloxane (PDMS) by spin coating a 1:1 by weight solution of Toluene : PDMS at 500 rpm so that all the wires were completely embedded in PDMS to avoid any damage to the tip while handling. The sample was heated on a hot plate at a temperature of 120^{0}C for 5 hours. The tapered wire arrays embedded in PDMS were peeled off the surface using a razor blade to obtain flexible films as shown in Figure 3 (a).

Simulation procedure for optical properties: Rigorous 3D full field electromagnetic wave FDTD simulations of tapered microwire arrays were performed using a commercial software package, Lumerical FDTD. The arrays were constructed using the 3D rectangular simulation region with periodic boundary conditions along x and y axes to depict 7μm square lattice of the arrays, and infinite boundary conditions rendered as perfectly matched layers (PML) along z axis. In the simulation region tapered microwires had a top diameter of 50nm, bottom diameter of 7μm, and height of 75μm. Palik material data provided by Lumerical was used for modelling the material as Si. Single wavelength infinite plane wave sources at four different wavelengths (400nm, 600nm, 800nm, and 1000nm) were used with a long pulse time of 50fs to simulate steady state behavior. Generation rate in these structures was calculated using built in CW-generation (continuous wave generation) rate analysis group was used to obtain electron hole pair generation profiles at steady state under illumination.

Implied V_{OC} calculation:

The model was implemented in Microsoft Excel, using VBA to iteratively solve the transcendental equations for steady state carrier concentration. Thickness, surface recombination velocity, Shockley-Reed-Hall lifetime [44], and auger lifetime [45] in the bulk were input parameters. The model included the effect of wire arrays via including surface area enhancement factor and light trapping enhancement factor of $4n^2$. Material parameters were input and recombination rates were calculated using the workbook. In order to calculate the carrier lifetime, implied V_{oc}, and limiting efficiency, generation was first calculated assuming simple Beer-Lambert absorption using the optical properties for silicon tabulated by Green at al. [46]. Next, recombination was calculated using the empirical model developed by Richter et al. to describe Auger recombination [47], surface and Shockley-Reed-Hall recombination were calculated as described in [48] using the input surface recombination velocity and bulk minority carrier lifetime as free parameters. Once steady state generation and recombination were calculated, the voltage was calculated from the excess minority carrier concentration, as described in Eq. 1. Finally, an efficiency was extracted using the total generation as the J_{sc} and calculating a fill factor using the empirical model for a device without series resistance or shunting developed by M.A. Green [49]. In this model an intrinsic doping density (n_i) of 9.7 x 10^9 cm^{-3}, donor doping density (N_d) of 10^{17} cm^{-3}, and radiative recombination coefficient (B_{rad}) of 4.7 x 10^{15} cm^3s^{-1} were used. This model provides an estimate for the absolute maximum achievable efficiency. It neglects resistances within the device.

AUTHOR INFORMATION.

Author Contributions

†These authors contributed equally (SY and HSE)

Corresponding Author

*Email: haa@caltech.edu.

Notes

The authors declare no competing financial interest

ACKNOWLEDGMENTS

This work was supported in part by the National Science Foundation (NSF) and the Department of Energy (DOE) under NSF CA No. EEC-1041895 (HSE and CTC), and Joint Center for Artificial Photosynthesis, a DOE Energy Innovation Hub, supported through the Office of Science of the U.S. Department of Energy under Award No. DE- SC0004993. Some of us (CTC, HAA) are also supported in part by the U.S. Department of Energy through the Bay Area Photovoltaic Consortium under Award Number DE-EE0004946. We thank Dennis Friedrich for his collaborations for microwave detected photoconductive decay measurements, Professor Shu Hu for stimulating discussions and Carol Garland for her assistance with transmission electron microscopy. This work benefited from use of the Applied Physics and Materials Science Department's Transmission Electron Microscopy Facility. Fabrication is performed in Kavli Nanoscience Institute (KNI) at Caltech and we thank KNI staff for their assistance during fabrication. Lumerical FDTD simulations for this research used resources of the National Energy Research Scientific Computing Center, a DOE Office of Science User Facility supported by the Office of Science of the U.S. Department of Energy under Contract No. DE-AC02-05CH11231.

REFERENCES

1. Shockley, W.; Queisser, H. J., Detailed Balance Limit of Efficiency of p-n Junction Solar Cells. *Journal of Applied Physics* **1961,** *32* (3), 510-519.
2. Tiedje, T.; Yablonovitch, E.; Cody, G. D.; Brooks, B. G., Limiting efficiency of silicon solar cells. *Electron Devices, IEEE Transactions on* **1984,** *31* (5), 711-716.
3. Green, M. A.; Emery, K.; Hishikawa, Y.; Warta, W.; Dunlop, E. D., Solar cell efficiency tables (version 47). *Progress in Photovoltaics: Research and Applications* **2016,** *24* (1), 3-11.
4. Taguchi, M.; Yano, A.; Tohoda, S.; Matsuyama, K.; Nakamura, Y.; Nishiwaki, T.; Fujita, K.; Maruyama, E., 24.7% Record Efficiency HIT Solar Cell on Thin Silicon Wafer. *Photovoltaics, IEEE Journal of* **2014,** *4* (1), 96-99.

5. Ortega, P.; Calle, E.; von Gastrow, G.; Repo, P.; Carrió, D.; Savin, H.; Alcubilla, R., High-efficiency black silicon interdigitated back contacted solar cells on p-type and n-type c-Si substrates. *Progress in Photovoltaics: Research and Applications* **2015,** *23* (11), 1448-1457.
6. Kowalczewski, P.; Bozzola, A.; Liscidini, M.; Claudio Andreani, L., Light trapping and electrical transport in thin-film solar cells with randomly rough textures. *Journal of Applied Physics* **2014,** *115* (19), 194504.
7. Yablonovitch, E., Statistical ray optics. *J. Opt. Soc. Am.* **1982,** *72* (7), 899-907.
8. Brendel, R.; Petermann, J. H.; Zielke, D.; Schulte-Huxel, H.; Kessler, M.; Gatz, S.; Eidelloth, S.; Bock, R.; Rojas, E. G.; Schmidt, J.; Dullweber, T., High-Efficiency Cells From Layer Transfer: A First Step Toward Thin-Film/Wafer Hybrid Silicon Technologies. *IEEE Journal of Photovoltaics* **2011,** *1* (1), 9-15.
9. Wang, L.; Lochtefeld, A.; Han, J.; Gerger, A. P.; Carroll, M.; Ji, J.; Lennon, A.; Li, H.; Opila, R.; Barnett, A., Development of a 16.8% Efficient 18-μm Silicon Solar Cell on Steel. *IEEE Journal of Photovoltaics* **2014,** *4* (6), 1397-1404.
10. Branham, M. S.; Hsu, W.-C.; Yerci, S.; Loomis, J.; Boriskina, S. V.; Hoard, B. R.; Han, S. E.; Chen, G., Silicon Solar Cells: 15.7% Efficient 10-μm-Thick Crystalline Silicon Solar Cells Using Periodic Nanostructures (Adv. Mater. 13/2015). *Advanced Materials* **2015,** *27* (13), 2268-2268.
11. Jeong, S.; McGehee, M. D.; Cui, Y., All-back-contact ultra-thin silicon nanocone solar cells with 13.7% power conversion efficiency. *Nat Commun* **2013,** *4*.
12. Brongersma, M. L.; Cui, Y.; Fan, S., Light management for photovoltaics using high-index nanostructures. *Nat Mater* **2014,** *13* (5), 451-460.
13. Raut, H. K.; Ganesh, V. A.; Nair, A. S.; Ramakrishna, S., Anti-reflective coatings: A critical, in-depth review. *Energy & Environmental Science* **2011,** *4* (10), 3779-3804.
14. (a) Berginski, M.; Hüpkes, J.; Gordijn, A.; Reetz, W.; Wätjen, T.; Rech, B.; Wuttig, M., Experimental studies and limitations of the light trapping and optical losses in microcrystalline silicon solar cells. *Solar Energy Materials and Solar Cells* **2008,** *92* (9), 1037-1042; (b) Jovanov, V.; Planchoke, U.; Magnus, P.; Stiebig, H.; Knipp, D., Influence of back contact morphology on light trapping and plasmonic effects in microcrystalline silicon single junction and micromorph tandem solar cells. *Solar Energy Materials and Solar Cells* **2013,** *110*, 49-57; (c) Depauw, V.; Meng, X.; Daif, O. E.; Gomard, G.; Lalouat, L.; Drouard, E.; Trompoukis, C.; Fave, A.; Seassal, C.; Gordon, I., Micrometer-Thin Crystalline-Silicon Solar Cells Integrating Numerically Optimized 2-D Photonic Crystals. *IEEE Journal of Photovoltaics* **2014,** *4* (1), 215-223.
15. Kelzenberg, M. D.; Boettcher, S. W.; Petykiewicz, J. A.; Turner-Evans, D. B.; Putnam, M. C.; Warren, E. L.; Spurgeon, J. M.; Briggs, R. M.; Lewis, N. S.; Atwater, H. A., Enhanced absorption and carrier collection in Si wire arrays for photovoltaic applications. *Nat Mater* **2010,** *9* (3), 239-244.
16. Kelzenberg, M. D.; Turner-Evans, D. B.; Putnam, M. C.; Boettcher, S. W.; Briggs, R. M.; Baek, J. Y.; Lewis, N. S.; Atwater, H. A., High-performance Si microwire photovoltaics. *Energy & Environmental Science* **2011,** *4* (3), 866-871.
17. Putnam, M. C.; Boettcher, S. W.; Kelzenberg, M. D.; Turner-Evans, D. B.; Spurgeon, J. M.; Warren, E. L.; Briggs, R. M.; Lewis, N. S.; Atwater, H. A., Si microwire-array solar cells. *Energy & Environmental Science* **2010,** *3* (8), 1037-1041.

18. Shearn, M.; Sun, X.; Henry, M. D.; Yariv, A.; Scherer, A., Advanced Plasma Processing: Etching, Deposition, and Wafer Bonding Techniques for Semiconductor Applications. In *Semiconductor Technologies*, Grym, J., Ed. InTech: 2010; pp 79-104.
19. Henry, M. D.; Walavalkar, S.; Homyk, A.; Scherer, A., Alumina etch masks for fabrication of high-aspect-ratio silicon micropillars and nanopillars. *Nanotechnology* **2009,** *20* (25), 255305.
20. Kern, W.; Puotinen, A. A., Cleaning Solutions Based on Hydrogen Peroxide for Use in Silicon Semiconductor Technology. *RCA review* **1970,** *31*, 187-206.
21. Liu, X.; Coxon, P. R.; Peters, M.; Hoex, B.; Cole, J. M.; Fray, D. J., Black silicon: fabrication methods, properties and solar energy applications. *Energy & Environmental Science* **2014,** *7* (10), 3223-3263.
22. Sainiemi, L.; Jokinen, V.; Shah, A.; Shpak, M.; Aura, S.; Suvanto, P.; Franssila, S., Non-Reflecting Silicon and Polymer Surfaces by Plasma Etching and Replication. *Advanced Materials* **2011,** *23* (1), 122-126.
23. Cho, S. J.; An, T.; Lim, G., Three-dimensionally designed anti-reflective silicon surfaces for perfect absorption of light. *Chemical Communications* **2014,** *50* (99), 15710-15713.
24. Plass, K. E.; Filler, M. A.; Spurgeon, J. M.; Kayes, B. M.; Maldonado, S.; Brunschwig, B. S.; Atwater, H. A.; Lewis, N. S., Flexible Polymer-Embedded Si Wire Arrays. *Advanced Materials* **2009,** *21* (3), 325-328.
25. Turner-Evans, D. B.; Emmer, H.; Chen, C. T.; Atwater, H. A., Flexible, Transparent Contacts for Inorganic Nanostructures and Thin Films. *Advanced Materials* **2013,** *25* (29), 4018-4022.
26. Akimov, Y. A.; Koh, W. S.; Ostrikov, K., Enhancement of optical absorption in thin-film solar cells through the excitation of higher-order nanoparticle plasmon modes. *Opt. Express* **2009,** *17* (12), 10195-10205.
27. Chow, E.; Lin, S. Y.; Johnson, S. G.; Villeneuve, P. R.; Joannopoulos, J. D.; Wendt, J. R.; Vawter, G. A.; Zubrzycki, W.; Hou, H.; Alleman, A., Three-dimensional control of light in a two-dimensional photonic crystal slab. *Nature* **2000,** *407* (6807), 983.
28. Joannopoulos, J. D.; Villeneuve, P. R.; Fan, S., Photonic crystals: putting a new twist on light. *Nature* **1997,** *386* (6621), 143-149.
29. Meade, J. D. J. S. G. J. J. N. W. R. D., *Photonic Crystals: Molding the Flow of Light*. 2nd ed.; Princeton University Press: Princeton, 2008.
30. Fountaine, K. T.; Kendall, C. G.; Atwater, H. A., Near-unity broadband absorption designs for semiconducting nanowire arrays via localized radial mode excitation. *Opt. Express* **2014,** *22* (9), A930-A940.
31. Grzela, G.; Paniagua-Domínguez, R.; Barten, T.; Fontana, Y.; Sánchez-Gil, J. A.; Gómez Rivas, J., Nanowire antenna emission. *Nano Lett.* **2012,** *12* (11), 5481-5486.
32. Cao, L.; Fan, P.; Vasudev, A. P.; White, J. S.; Yu, Z.; Cai, W.; Schuller, J. A.; Fan, S.; Brongersma, M. L., Semiconductor nanowire optical antenna solar absorbers. *Nano Lett.* **2010,** *10* (2), 439-445.
33. Fountaine, K. T.; Whitney, W. S.; Atwater, H. A.; Ieee, Achieving Near-Unity Broadband Absorption in Sparse Arrays of GaAs NWs via a Fundamental Understanding of Localized Radial Modes. *2014 Ieee 40th Photovoltaic Specialist Conference (Pvsc)* **2014**, 3507-3509.
34. Fountaine, K. T.; Whitney, W. S.; Atwater, H. A., Resonant absorption in semiconductor nanowires and nanowire arrays: Relating leaky waveguide modes to Bloch photonic crystal modes. *J. Appl. Phys.* **2014,** *116* (15), 6.

35. Garnett, E.; Yang, P. D., Light Trapping in Silicon Nanowire Solar Cells. *Nano Lett.* **2010,** *10* (3), 1082-1087.
36. Cao, L. Y.; White, J. S.; Park, J. S.; Schuller, J. A.; Clemens, B. M.; Brongersma, M. L., Engineering light absorption in semiconductor nanowire devices. *Nat. Mater.* **2009,** *8* (8), 643-647.
37. Abujetas, D. R.; Paniagua-Dominguez, R.; Sanchez-Gil, J. A., Unraveling the Janus Role of Mie Resonances and Leaky/Guided Modes in Semiconductor Nanowire Absorption for Enhanced Light Harvesting. *ACS Photonics* **2015,** *2* (7), 921-929.
38. Anttu, N.; Xu, H. Q., Coupling of Light into Nanowire Arrays and Subsequent Absorption. *J. Nanosci. Nanotechnol.* **2010,** *10* (11), 7183-7187.
39. Love, A. W. S. J., *Optical Waveguide Theory*. Spring Science & Business Media: 2012.
40. Savin, H.; Repo, P.; von Gastrow, G.; Ortega, P.; Calle, E.; Garín, M.; Alcubilla, R., Black silicon solar cells with interdigitated back-contacts achieve 22.1% efficiency. *Nat Nano* **2015,** *10* (7), 624-628.
41. Kerschaver, E. V.; Beaucarne, G., Back-contact solar cells: a review. *Progress in Photovoltaics: Research and Applications* **2006,** *14* (2), 107-123.
42. Wang, S.; Weil, B. D.; Li, Y.; Wang, K. X.; Garnett, E.; Fan, S.; Cui, Y., Large-Area Free-Standing Ultrathin Single-Crystal Silicon as Processable Materials. *Nano Letters* **2013,** *13* (9), 4393-4398.
43. (a) Ardo, S.; Park, S. H.; Warren, E. L.; Lewis, N. S., Unassisted solar-driven photoelectrosynthetic HI splitting using membrane-embedded Si microwire arrays. *Energy & Environmental Science* **2015,** *8* (5), 1484-1492; (b) Maiolo, J. R.; Kayes, B. M.; Filler, M. A.; Putnam, M. C.; Kelzenberg, M. D.; Atwater, H. A.; Lewis, N. S., High Aspect Ratio Silicon Wire Array Photoelectrochemical Cells. *Journal of the American Chemical Society* **2007,** *129* (41), 12346-12347; (c) Walter, M. G.; Warren, E. L.; McKone, J. R.; Boettcher, S. W.; Mi, Q.; Santori, E. A.; Lewis, N. S., Solar Water Splitting Cells. *Chemical Reviews* **2010,** *110* (11), 6446-6473; (d) Boettcher, S. W.; Warren, E. L.; Putnam, M. C.; Santori, E. A.; Turner-Evans, D.; Kelzenberg, M. D.; Walter, M. G.; McKone, J. R.; Brunschwig, B. S.; Atwater, H. A.; Lewis, N. S., Photoelectrochemical Hydrogen Evolution Using Si Microwire Arrays. *Journal of the American Chemical Society* **2011,** *133* (5), 1216-1219; (e) Warren, E. L.; Atwater, H. A.; Lewis, N. S., Silicon Microwire Arrays for Solar Energy-Conversion Applications. *The Journal of Physical Chemistry C* **2014,** *118* (2), 747-759.
44. Shockley, W.; Read, W. T., Statistics of the Recombinations of Holes and Electrons. *Physical Review* **1952,** *87* (5), 835-842.
45. Auger, P., Sur les rayons β secondaires produits dans un gaz par des rayons X. *C.R.A.S.* **1923,** *177*.
46. Green, M. A.; Keevers, M. J., Optical properties of intrinsic silicon at 300 K. *Progress in Photovoltaics: Research and Applications* **1995,** *3* (3), 189-192.
47. Richter, A.; Glunz, S. W.; Werner, F.; Schmidt, J.; Cuevas, A., Improved quantitative description of Auger recombination in crystalline silicon. *Physical Review B* **2012,** *86* (16), 165202.
48. Simon M. Sze, K. K. N., *Physics of Semiconductor Devices*. 3 ed.; John Wiley & Sons, Inc.: United States of America, 2007; p 832.
49. Green, M. A., Accuracy of analytical expressions for solar cell fill factors. *Solar Cells* **1982,** *7* (3), 337-340.

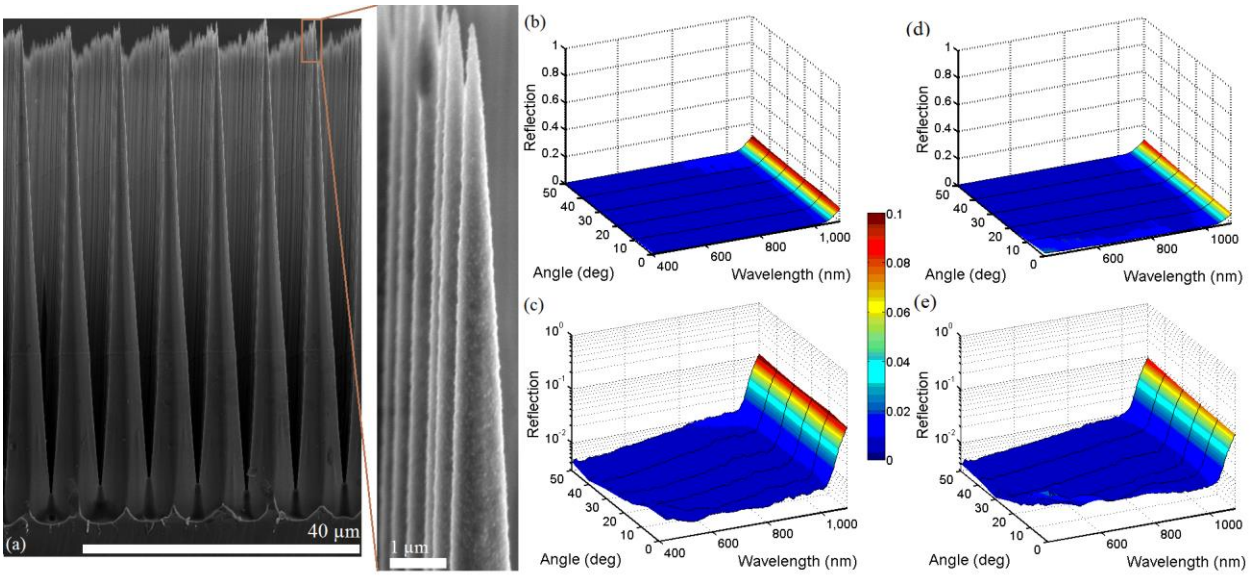

Figure 1: (a) Si substrates with tapered microwire arrays etched via ICPRIE. The inset shows the morphology of the tip of a tapered microwire, (b) and (c) show the reflectance (0.98%) of Si substrates with tapered microwire arrays measured using an integrating sphere plotted on a linear scale and log scale respectively. (d) and (e) show the reflectance (0.97%) of the arrays with a SiNx anti-reflection coating

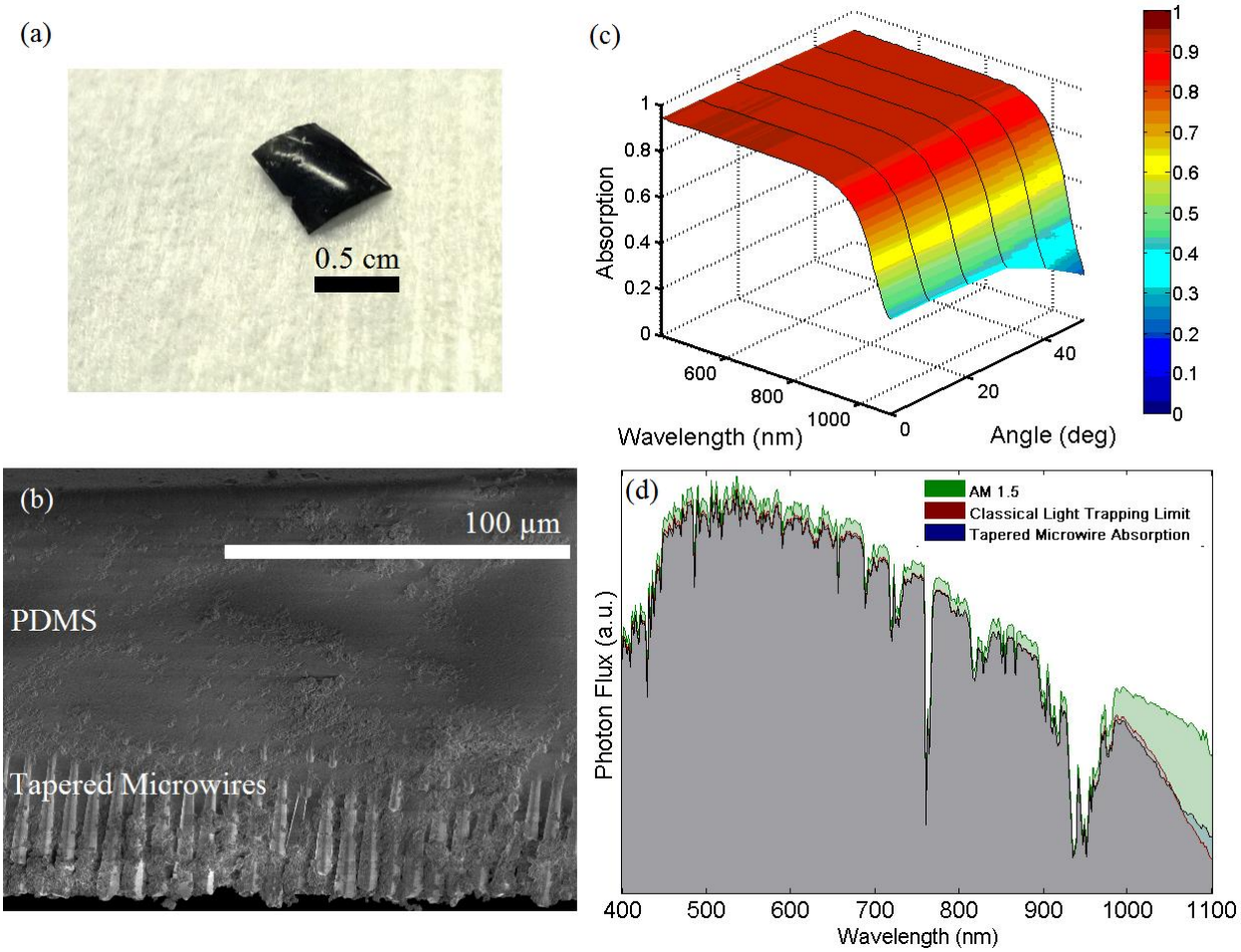

Figure 2: (a) Optical photograph of the films with tapered microwires embedded in PDMS, (b) cross section SEM of the film, (c) absorption measured in the film in the range 400nm – 1100nm while varying the angle of incidence from 0^0 to 50^o, and (d) comparison of absorbed photon flux at normal incidence with classical light trapping limit absorption of a 20 µm thick slab

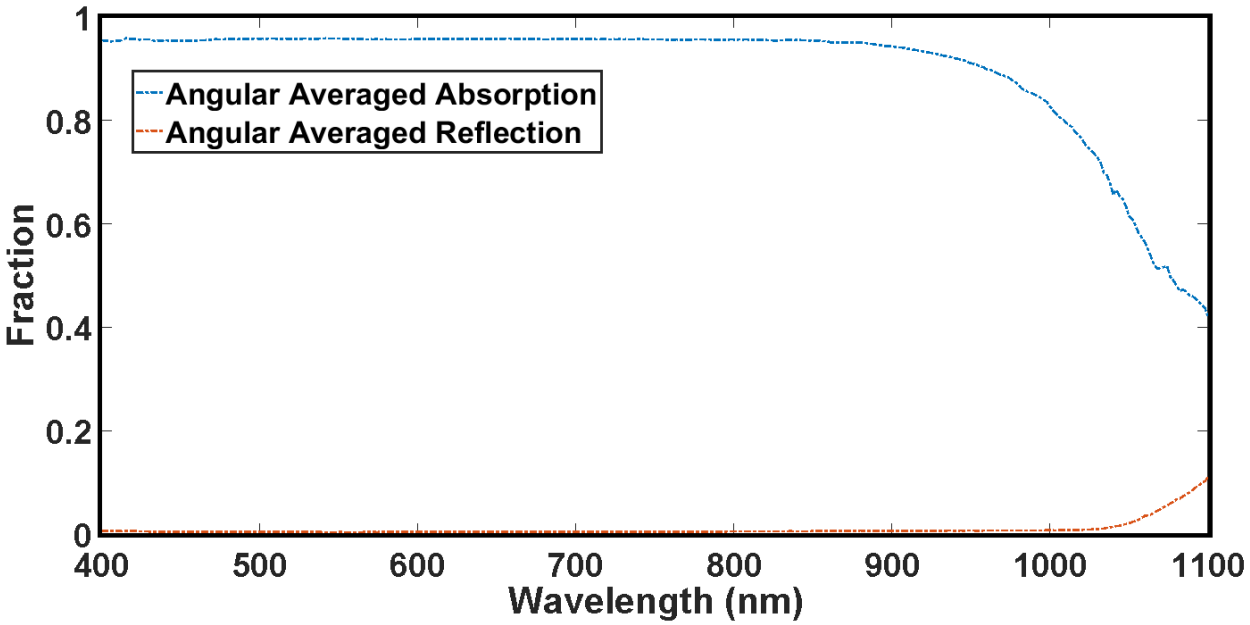

Figure 3: Plot of angular averaged reflection from Si substrate with tapered microwires etched into it is shown in red, and in blue is the plot of angular averaged absorption in tapered microwire arrays embedded in PDMS

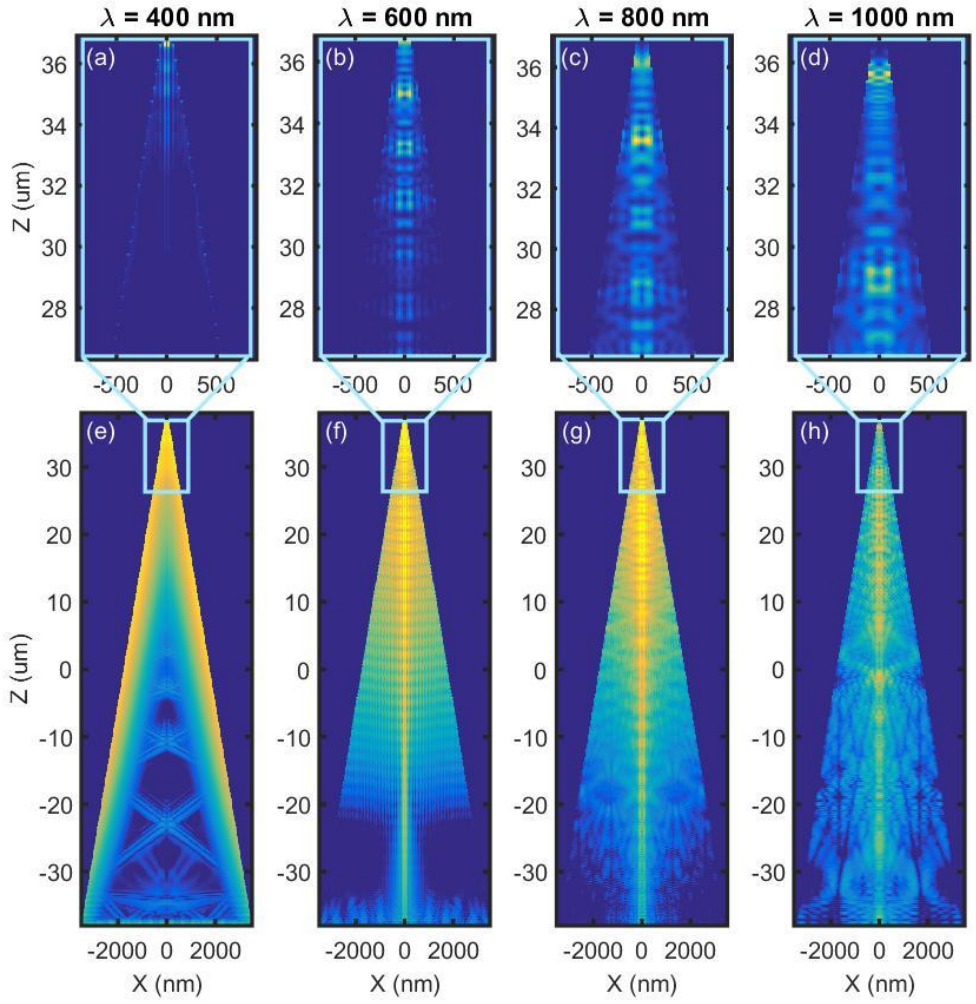

Figure 4: Longitudinal cross sections of power absorption for Si microwires at 400 (a,e), 600 (b,f), 800 (c,g), and 1000 (d,h) nm wavelengths, respectively; (a-d) upper portion of microwire with linear intensity scale; (e-h) complete microwire with logarithmic intensity scale; light blue squares correspond to expanded cross sections in (a-d); different relative scales are used for each figure to highlight modes

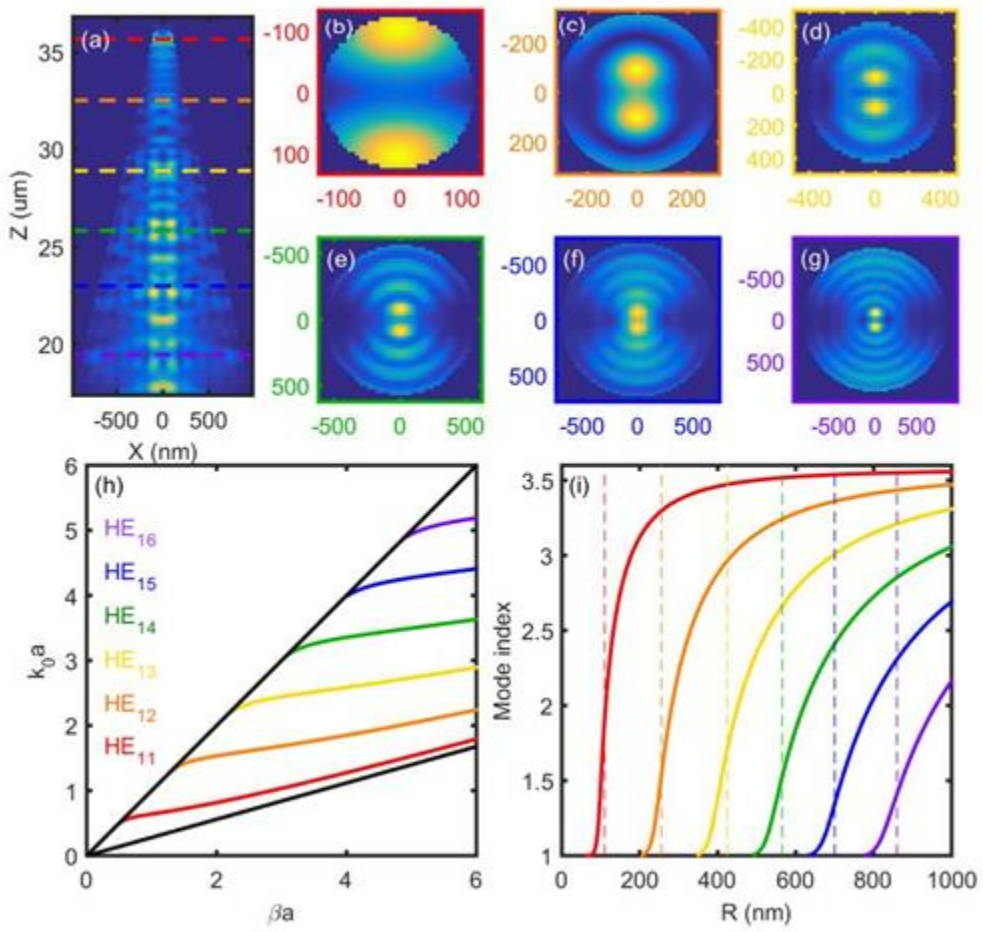

Figure 5: Detailed mode analysis of upper portion of a tapered microwire at λ=1000nm; mode color key in (h) is applied throughout the figure; (a) longitudinal absorption cross section with dashed lines indicating radial cross sections; (b-g) radial cross sections, exhibiting HE_{1n} modes; (h) traditional dispersion curves for HE_{1n} modes for n=3.577; (i) non-traditional dispersion curves, converted from (h) for λ=1000nm.